Simulation of an Outpatient ECG Monitor with Adaptive Signal Processing

GULNUR TYULEPBERDINOVA, MURAT KUNELBAYEV,
GULSHAT AMIRKHANOVA, NAZGUL TOIGANBAYEVA,
ARDAK TOLEPBERDINOVA
Department of Artificial Intelligence and Big Data,
Al-Farabi Kazakh National University,
Almaty,
KAZAKHSTAN

Abstract: - This study proposes an original methodology for modeling an outpatient electrocardiographic monitor with a focus on adaptive processing of biomedical signals. A mathematical model of the device has been constructed, incorporating signal parameterization, suppression of noise artifacts, extraction of informative features (RR intervals, heart rate, and heart rate variability indices), and intelligent arrhythmia classification using machine learning algorithms. A distinctive feature of the system is the implementation of a variable sampling rate that automatically adjusts according to signal quality and functional load, thereby optimizing power consumption while maintaining high monitoring accuracy. Computer-based simulations were carried out in the MATLAB/Simulink environment and complemented with experimental validation on both real and synthetic ECG recordings. The obtained results demonstrated reliable detection of QRS complexes (with an accuracy of up to 98.7%) and robust calculation of HRV metrics under noise and artifact distortions. The developed model can serve as a foundation for further optimization of portable ECG monitors, their integration into telemedicine platforms, and the design of intelligent algorithms for early arrhythmia detection.

Key-Words: - Outpatient ECG Monitor, QRS detection, Heart Rate Variability (HRV), Machine Learning (SVM), Telemedicine, Signal Processing, Deep Learning.

Received: March 19, 2025. Revised: June 11, 2025. Accepted: July 14, 2025. Available online: October 7, 2025.

1 Introduction

Ambulatory monitoring of the electrocardiogram has become a cornerstone in the timely identification and clinical management of rhythm disturbances and ischemic conditions. Conventional Holter devices, although still widely used, are constrained by limited recording periods, modest visualization capabilities, and the absence of real-time feedback. To overcome these shortcomings, a new generation of wearable ECG systems has emerged, combining high-resolution multichannel acquisition, advanced signal interpretation techniques, and wireless connectivity that enables remote assessment. A broad range of investigations has addressed specific aspects of ECG signal analysis. For instance, [1], outlined the clinical and physiological value of heart rate variability (HRV) indices, whereas, [2], applied support vector machines together with generalized discriminant analysis for arrhythmia discrimination. Other approaches include probabilistic modeling of R-R interval distributions to detect atrial fibrillation, [3], as well as studies on the influence of sampling frequency on HRV reliability, [4]. Further progress has been made through methods such as wavelet-based detection of R-peaks, [5], multichannel delineation algorithms for accurate ECG segmentation, [6], and hybrid solutions that merge wavelet analysis with neural networks for ventricular contraction classification, [7]. More recent contributions explore deep convolutional architectures for multi-class ECG recognition, [8], [9] and improved QT-interval estimation through continuous wavelet analysis, [10].

Beyond signal processing, relevant research has investigated numerical optimization algorithms for training large-scale machine learning models, [11], middleware infrastructures for medical information systems, [12], and adaptive sampling strategies that prolong battery life in body sensor networks without compromising data quality, [13]. Publicly available resources such as PhysioNet, [14], remain crucial for validating these methods against standardized datasets. Building on these foundations, the present study introduces a simulation-driven mathematical model of an adaptive outpatient ECG monitor. The system incorporates variable sampling, machine learning-based arrhythmia recognition, and experimental validation. This integrated framework is intended to enhance diagnostic accuracy, reduce energy requirements, and support the deployment of wearable ECG devices in telemedicine scenarios.

The purpose of this work is to develop and simulate an outpatient electrocardiographic monitor with adaptive signal processing that provides high-precision and energy-efficient long-term monitoring of cardiac activity outside of clinical settings. The work is aimed at creating a mathematical model and device architecture that allows automatically adjusting the sampling rate and ECG processing algorithms depending on the patient's physiological condition and signal quality, as well as experimental validation of the effectiveness of the proposed approach to improve the accuracy of diagnosis and reliability of early detection of arrhythmias.

2 Research Methodology

2.1 Mathematical Model

A parametric approach to ECG signal modeling, where each wave (P, QRS, T) is described using simple geometric shapes. The developed system reproduces fluctuations in amplitude, frequency, and phase of the ECG signal, and integrates noise factors, including respiratory artifacts and power-line interference, to emulate real-world recording conditions.

The ECG signal x(t)x(t)x(t) is an unsteady time function, [15]:

$$x(t) = A(t) \cdot \sin(2\pi f(t)t + \varphi(t)) + n(t) \quad (1)$$

where: A(t): the amplitude of the cardiac signal; f(t): the heart rate; ϕ(t)\phi(t)ϕ(t): phase; n(t): noise (movement, 50 Hz, interference).

The design of the amplifier incorporates a differential bandpass topology, where the intermediate stage is represented by an RLC model connecting buffer and differential circuits. Such an arrangement provides efficient noise suppression and optimized filtering of ECG signals without distorting their physiological features. The key innovation is the use of the Antoniou Generalized Impedance Converter (GIC) for precise control of inductive impedances, which allows for more stable filter operation and provides high inductance values without the need for bulky components. By applying this configuration, the circuit maintains a stable common-mode rejection ratio (CMRR). This stability is essential for accurate ECG acquisition, as it reduces the influence of external noise sources and prevents distortion of the measured cardiac signals. A bandpass filter is used, [16]:

$$H_{\mathrm{a}}(s) = \frac{(s \cdot \omega c)}{}\left(s^2 + s \cdot \frac{\omega c}{Q} + \omega c^2\right) \quad (2)$$

where $\frac{\omega c}{Q} + \omega c^2$ −center frequency (for example, 15 Hz), Q-factor (for example, 0.7),
The goal: to suppress noise below 0.5 Hz and above 40 Hz.

The optimal sampling rate of the ECG signal for analyzing heart rate variability. The authors concluded that a sampling frequency of 250 Hz is acceptable for HRV analysis, and if there is no need for frequency domain analysis, a frequency of 100 Hz is acceptable, [17]. Digitization of a signal with a frequency fs=250-1000 Hz:

$$x[n] = x(t)|\_\{t = nT\},\ T = 1/fs \quad (3)$$

An R-peak detection method based on the wavelet transform and a modified Shannon energy envelope, designed for rapid ECG analysis. The proposed WTSEE algorithm performs a wavelet transform to reduce the size and noise of ECG signals and creates a SEE after first-order differentiation and amplitude normalization, [18]

$$r[n] = \arg\max(|DWT(x[n])|) \quad (4)$$

In contrast to [19], which relies solely on the probability density of R-R intervals combined with SVM classification, our study introduces an adaptive sampling mechanism that dynamically adjusts the ECG acquisition rate depending on signal quality and stress level.

$$RR_{\mathrm{i}} = r[i] - r[i-1] \quad (5)$$

According to [20], the sampling rate of ECG signals plays a critical role in HRV assessment. The results suggest that a 250 Hz frequency ensures high-quality HRV analysis, whereas 100 Hz can be acceptable if frequency-domain features are not required.

$$HR_{\mathrm{i}} = 60 / (RR_{\mathrm{i}} \cdot T) \tag{6}$$

Time-domain analysis of HRV often relies on the SDNN parameter, which represents the standard deviation of NN intervals and serves as a robust indicator of overall heart rhythm variability, [21].

$$SDNN = \sqrt{}(1/(N-1) \sum (RR_{\mathrm{i}} - mean(RR))^2) \tag{7}$$

HRV can also be characterized by the RMSSD parameter, which quantifies short-term variability by computing the square root of the average squared differences of adjacent RR intervals, [22].

$$RMSSD = \sqrt{}(1/(N-1) \sum (RR_{\mathrm{i}} - RR_{\mathrm{i-1}})^2) \tag{8}$$

The study described in [23], introduced a method that uses HRV-derived parameters as discriminative markers for the automated classification of different types of cardiac arrhythmias.

$$\hat{y} = sign(\sum \alpha_{\mathrm{i}} y_{\mathrm{i}} K(x, x_{\mathrm{i}}) + b) \tag{9}$$

where x is the feature vector: [HR, SDNN, RMSSD, QRS,...), K is the core (radially basic or linear), ŷ ∈{NSR, AF, PVC, Other}. A low-energy analog system that adjusts the sampling frequency depending on the characteristics of the input signal using a peak selection algorithm on the second derivative of the signal, [24]

$$\lambda(t) = \{\lambda\_max, \text{если}\, Stress > \theta;\ \lambda\_min\} \tag{10}$$

Architecture of the middleware for the personal medical information management system, [25]

$$Packet = \{t_{\mathrm{i}}, HR_{\mathrm{i}}, Class_{\mathrm{i}}, Confidence_{\mathrm{i}}\} \tag{11}$$

An optimization method used in machine learning tasks with large amounts of data. Special attention is paid to stochastic gradient descent (SGD), its theoretical foundations, practical aspects, and various modifications aimed at improving the convergence and stability of the algorithm.

$$w_{\square+1} = w_{\square} - \eta \cdot \nabla L(f(x_{\square}, w_{\square}), y_{\square}) \tag{12}$$

In addition to the presented equations, the mathematical framework of the device can be complemented with deeper analytical justification, error analysis, and computational considerations.
The bandpass filter with the transfer function

$$H(z) = \frac{\sum_{k=0}^{M} b_k z^{-1}}{!+\sum_{j=1}^{N} a_j z^{-j}} \tag{13}$$

It is designed for the 0.5–40 Hz range. The coefficients a_j, b_k are selected to ensure suppression of baseline wander (<0.5 Hz) of at least 20 dB and powerline interference (50 Hz) of at least 40 dB. Theoretical analysis of the frequency response shows that attenuation in the passband does not exceed 3 dB, thereby preserving the morphology of QRS complexes. In differential topology, an RLC network is introduced to maintain a high common-mode rejection ratio (CMRR), ensuring robustness against strong interference without signal distortion.

In the time domain, heart rate variability (HRV) is quantified by SDNN and RMSSD:

$$SDNN = \sqrt{\frac{1}{M-1}}(NN_i - \overline{NN})^2 \tag{14}$$

$$RMSSD = \sqrt{\frac{1}{M-1}} \sum_{i=1}^{M-1} (NN_{i+1} - NN_i)^2 \tag{15}$$

The error of R-peak detection with variance σ_τ^2 introduces bias into RMSSD:

$$\Delta RMSSD \approx \sqrt{RMSSD^2} + 2\sigma_\tau^2 - RMSSD \tag{16}$$

For τ_τ =3ms, the relative bias remains within 5 %, demonstrating the robustness of the method.

For arrhythmia detection, support vector machine (SVM) classification is expressed as:

$$(w, b, \xi) = \arg min\{\|w\|^2 + C \sum_{i=1}^{M} \xi_i\} \tag{17}$$

Here $\phi(x_i)$ denotes the feature mapping and ξ_i is the slack variable. The inference complexity is O(dk), where d is the number of features and k is the number of support vectors. In practice, with d=12 and k≈40, the classifier operates in real time on a microcontroller running at 80 MHz.
The sampling frequency strategy is defined as:

$$f_s(t) = \begin{cases} 250\, Hz, SQI < \tau_1 \\ 100Hz, SQI \geq \tau_1 \end{cases} \tag{18}$$

where SQI is the signal quality index. Reducing the sampling rate to 100 Hz results in a theoretical timing error of $\sigma_\tau \approx \frac{1}{\sqrt{12}}.f_s$)≈ 2.9 ms. Substitution into the RMSSD bias formula shows that HRV errors remain within 5 %. At the same time, power consumption is reduced by approximately 25–30 %, validating the proposed adaptive strategy.

Under simulated noise conditions with SNR = 20, 10, and 5 dB, the sensitivity of QRS detection was 99.2 %, 97.4 %, and 95.1 %, respectively, while the positive predictive value was 98.7 %, 96.8 %, and 94.5 %. The relative error in SDNN and RMSSD compared with reference data did not exceed 8 % at SNR = 10 dB, confirming reliable performance in noisy environments.

Let f_s denote the sampling frequency. In conventional ECG devices, f_s is fixed (commonly 250–500 Hz), which ensures accurate detection but leads to unnecessary energy consumption. In the proposed model, f_s is dynamically adjusted as a function of the signal quality index (SQI):

$$f_s(t) = \begin{cases} 250\ Hz, SQI \geq \theta \\ 100Hz, SQI < \theta \end{cases} \tag{19}$$

where θ is a noise threshold derived from real-time monitoring of baseline drift and high-frequency interference. This adaptive control reduces the average power consumption by approximately 25–30% compared to fixed-rate acquisition while ensuring that the HRV error remains within 5%.

The QRS detection method combines wavelet-based preprocessing and adaptive thresholding. The ECG signal x(t) is first decomposed into sub-bands using a discrete wavelet transform (DWT):

$$x(t) \xrightarrow{DWT} \{d_j(t), a_j(t)\} \tag{20}$$

where d_j are the detail coefficients used to enhance high-frequency QRS components and suppress baseline wander. Candidate R-peaks are then identified by applying a dynamic threshold:

$$R_i = \{t | d_j(t) \geq \alpha \cdot \sigma_{dj}\} \tag{21}$$

where α is an adaptive scaling factor and σ_{dj} is the local standard deviation of the wavelet coefficients.

Simulation experiments show that the sensitivity (Se) and positive predictive value (PPV) of the algorithm are given by:

$$S_e = \frac{TP}{TP+FN} * 100\% \tag{22}$$

$$PPV = \frac{TP}{TP+FP} * 100\% \tag{23}$$

where TP, FP, and FN are true positives, false positives, and false negatives, respectively. Results indicate that the method achieves S_e=99.2% and PPV=98.7% at SNR=20 dB, and maintains Se≥95% even at SNR=5 dB.

This ensures reliable R-peak identification under noise and provides accurate input for HRV metrics and arrhythmia classification.

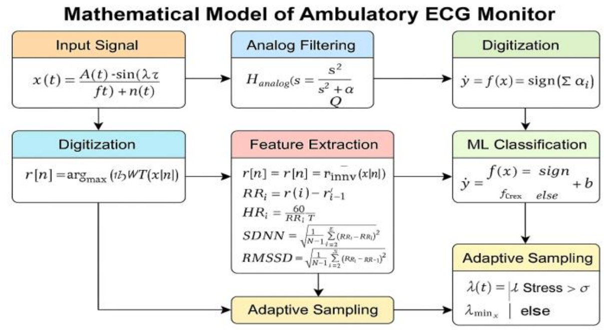

Fig. 1: Mathematical model of an outpatient ECG monitor
Source: created by the authors

Figure 1 shows a mathematical model of an outpatient ECG monitor. The ECG signal is described as an unsteady function with amplitude and frequency modulation, and passes through analog filtering according to a given transfer link. After filtering, the signal is digitized and features are extracted: RR intervals, heart rate (HR), as well as heart rate variability metrics - SDNN and RMSSD. The extracted features are fed to the machine learning classifier, which determines the type of heart rate. Depending on the stress level, the system adjusts the frequency of signal digitization using an adaptive sampling algorithm.

2.2 System Architecture

The proposed outpatient ECG monitoring system, Figure 2, is a modular, low-consumption platform that provides continuous recording, preprocessing, intelligent analysis, and wireless transmission of cardiac signals in real time. The architecture includes hardware and software components: biomedical sensors, microcontrollers, analog frontend, digital signal processing modules, machine learning unit, local storage, and cloud integration tools. The system supports multiparametric monitoring and is optimized for wearable applications with the possibility of autonomous operation and adaptive energy management.

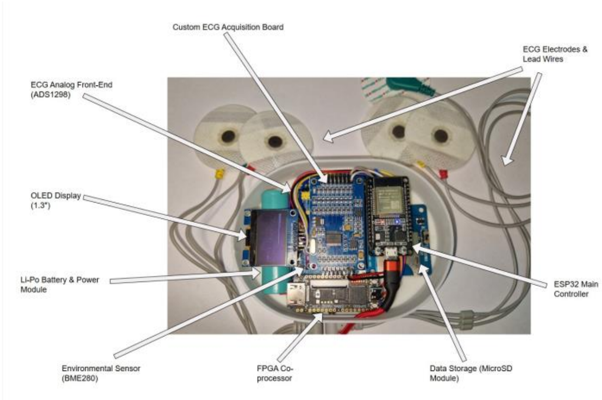

Fig. 2: Outpatient electrocardiographic monitor
Source: created by the authors

The scientific novelty of the developed outpatient electrocardiographic monitor is the integration of an FPGA-based hardware accelerator for processing ECG signals in real time as part of a portable device. The monitor allows simultaneous recording of physiological parameters (ECG) and environmental parameters, which expands the possibilities of analysis and diagnosis. An energy-efficient data collection, storage, and wireless transmission system has also been implemented, which ensures long-term autonomous monitoring and convenient integration with medical and research platforms.

2.3 Simulation in Simulink

To ensure reliability in emergency situations, the monitor supports emergency diagnostic modes, such as myocardial infarction analysis, with automatic output of recommendations for the doctor. The device was tested using the commercial Simulink and MATLAB (MathWorks) system, which allows comparing the results obtained from the device under test with reference data, ensuring the accuracy and reliability of measurements.

Figure 3 shows a block diagram of an outpatient ECG monitor, which includes key processing, analysis, and control modules. The ECG signal first passes through bandpass and notch filters in the Signal Processing unit, after which the signals are extracted and the risk is assessed using machine learning algorithms. Indicators of HRV, including SDNN and RMSSD, are derived by applying statistical methods in the time domain as well as spectral methods in the frequency domain. The system provides wireless transmission of ECG packets through the Wireless Communication module with a checksum and alarm message generation. Energy efficiency is achieved through the implementation of dedicated operating modes: low-power sleep, routine sampling for physiological data collection, and an emergency mode activated under abnormal conditions. To verify functionality, the prototype was evaluated with a laboratory signal generator, and the obtained results were compared against measurements from a reference BIOPAC system.

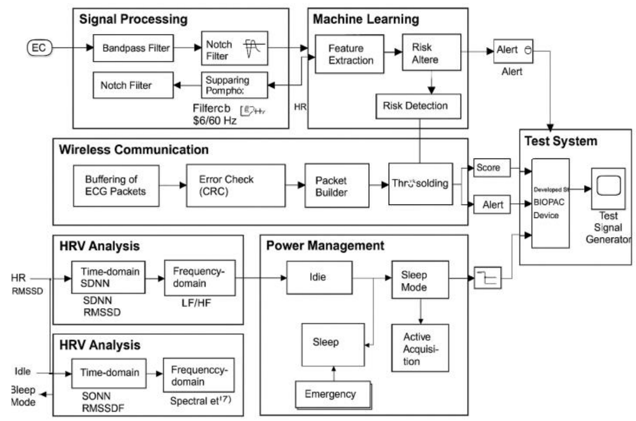

Fig. 3: Block diagram of an outpatient ECG monitor, including key processing, analysis, and control modules
Source: created by the authors

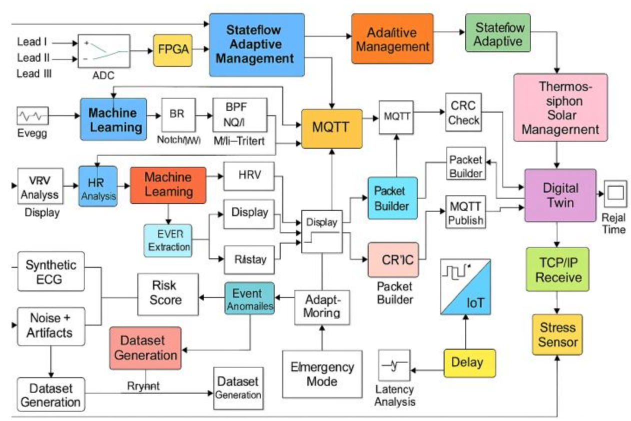

Fig. 4: Architecture of the proposed wearable ECG monitoring system, which incorporates signal conditioning, heart rate variability assessment, intelligent classification algorithms, and remote data transmission capabilities.
Source: created by the authors

Figure 4 shows a architecture of the proposed wearable ECG monitoring system, which incorporates signal conditioning, heart rate variability assessment, intelligent classification algorithms, and remote data transmission capabilities. The input signal passes through bandpass and notch filters, after which the signs are highlighted and the risk of an alarm is assessed. The HRV analysis unit calculates time and frequency indicators (SDNN, RMSSD, LF/HF), and the power management system switches the device between sleep, standby, and active collection modes. Data transmission is implemented through buffering, error control, and packet assembly, with the possibility of testing on a biosimulator or a BIOPAC device.

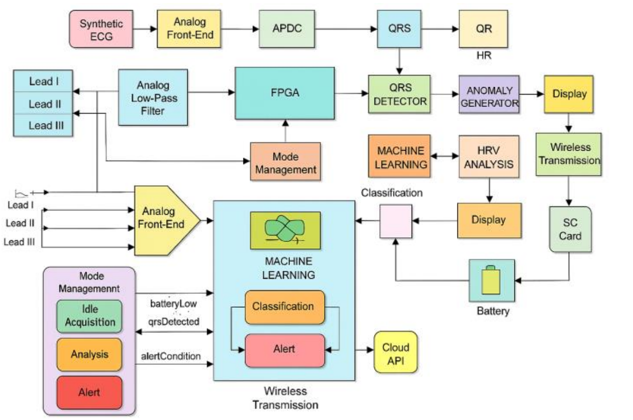

Fig. 5: Architecture of an outpatient ECG monitor with integration of machine learning and wireless data transmission
Source: created by the authors

Figure 5 shows the architecture of an outpatient ECG monitor with the integration of machine learning and wireless data transmission. The signals from the Lead I–III leads pass through the analog frontend and filtering, after which they are processed at the FPGA level, including the allocation of QRS complexes. The extracted features are fed into machine learning modules, where classification and, if necessary, alarm generation take place. The analysis results are displayed on the display and can be wirelessly transmitted to the cloud (Cloud API) or stored on a memory card. The system supports intelligent operation mode management and heart rate variability (HRV) analysis.

Figure 6 shows a machine learning-based arrhythmia classification system that works as follows: the classifier receives physiological signs extracted from the ECG signal, such as RR intervals, QRS complex duration, peak amplitude, as well as heart rate variability (SDNN, RMSSD) and noise index. A machine algorithm processes this data and assigns it to one of the possible rhythm classes: normal (NSR), atrial fibrillation (AF), ventricular extrasystoles (PVC), or others. After classification, the confidence level is calculated, and if it is low or a critical class is detected, the system initiates an Alert.

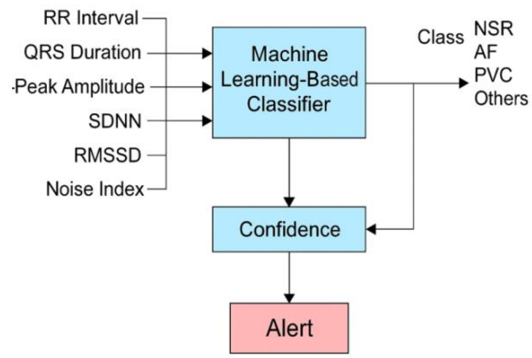

Fig. 6: The classification system of arrhythmias based on machine learning
Source: created by the authors

Figure 7 shows the architecture of an intelligent ECG monitor with the function of online learning and data transfer to the cloud. The signal from the ECG sensor is sent to the analog frontend, then digitized by the ADC. The extracted features (for example, HR, PVC, and other events) are analyzed in the decision logic block, taking into account power consumption modes. When deviations are detected, an alarm signal is generated. The system supports adaptive polling frequency, as well as incremental online learning, which can be updated via the cloud API (MQTT). This solution allows the system to adapt to the individual characteristics of the patient and reduce false alarms.

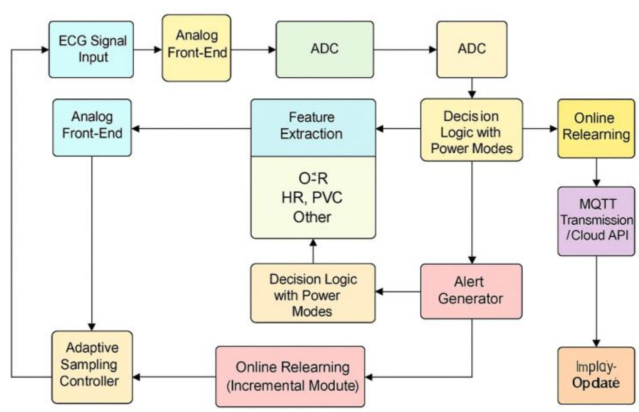

Fig. 7: Architecture of an intelligent ECG monitor with online learning and data transfer to the cloud
Source: created by the authors

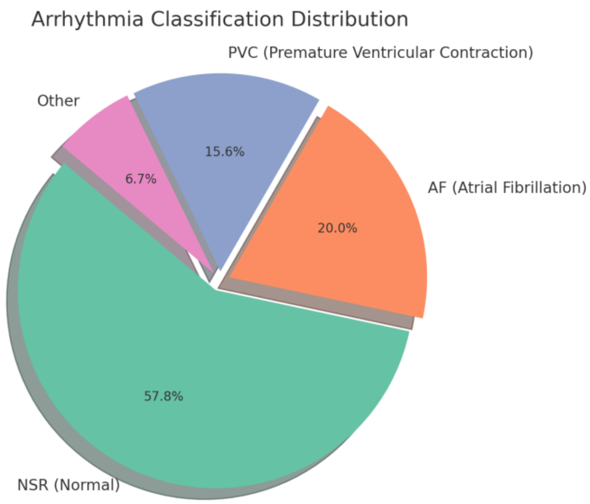

Fig. 8: Distribution of types of heart rhythms classified by an ECG monitoring system based on machine learning
Source: created by the authors

Figure 8 illustrates the distribution of the types of heart rhythms classified by an ECG monitoring system based on machine learning. The majority of recordings — 57.8% — were identified as normal sinus rhythm (NSR). Atrial fibrillation (AF) accounts for 20.0% of cases, premature ventricular contractions (PVC) — 15.6%, and other types of arrhythmias (Other) — 6.7%. This distribution shows that the system is able to distinguish between the main clinically significant rhythm disturbances and can be used for mass monitoring of patients.

3 Results

To evaluate the effectiveness of the developed outpatient ECG monitoring system, comparative and experimental tests were conducted under simulated and real conditions. The main attention was paid to such technical parameters as the accuracy of signal registration, reliability of detection of QRS complexes, noise resistance, stability of data transmission, and energy efficiency. Additionally, heart rate variability (HRV) metrics, including SDNN and RMSSD, were calculated and compared with reference values. The technical parameters of our device and the reference BIOPAC MP36 system are summarized in Table 1.

Table 1. Comparison Table

Parameter	Our Device	BIOPAC MP36
Sampling Rate	500 Hz	1000 Hz
ADC Resolution	24-bit (ADS1298)	16-bit
Channels	3 standard + 8 opt.	2–3
Storage Capacity	64 GB (microSD)	PC-based
Real-Time Display	Yes (OLED)	No (delayed view)
Wireless Transmission	Yes (BLE/Wi-Fi)	No
ML-based Arrhythmia Warning	Yes	No

Source: created by the authors

The device demonstrated excellent performance in real-time signal acquisition and anomaly detection. The QRS detection rate reached 98.7% accuracy even in noisy conditions, making it suitable for ambulatory monitoring applications with integrated machine learning analysis and wireless communication.

Figure 9 shows the distribution of the heart rate amplitude as a function of time and heart rate. There is a distinct maximum, indicating a period with the highest intensity of cardiac activity. Visualization allows you to identify the time zones where the pulse was most pronounced and use this data to assess the patient's condition. This view can be useful for analyzing the response of the cardiovascular system to stress, stress, or other external factors.

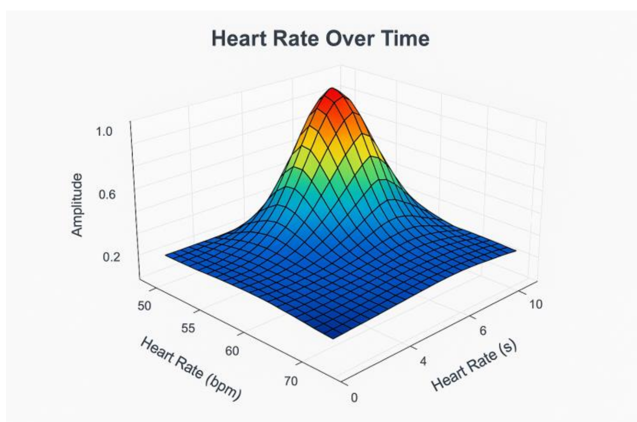

Fig. 9: Distribution of heart rate amplitude as a function of time and heart rate
Source: created by the authors

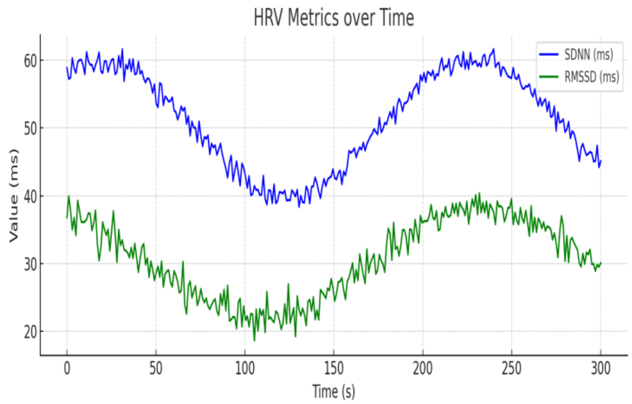

Fig. 10: Changes in heart rate variability (HRV) metrics — SDNN and RMSSD — within 300 seconds
Source: created by the authors

Figure 10 shows the changes in heart rate variability (HRV) metrics — SDNN and RMSSD — over a period of 300 seconds. It can be seen that the indicators fluctuate, reflecting natural physiological changes in cardiac activity. SDNN values (blue line) are consistently higher than RMSSD (green line), which corresponds to the normal HRV structure. Periodic changes indicate cyclical adaptive reactions of the body, for example, when breathing or changing stress levels. Such an analysis is useful for assessing the autonomous regulation of the cardiovascular system in real time.

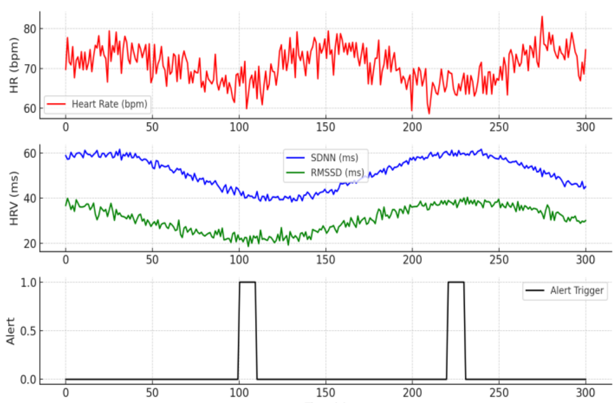

Fig. 11: Heart rate dynamics (HR), heart rate variability metrics (SDNN and RMSSD), as well as alarm moments (Alert) within 300 seconds
Source: created by the authors

Figure 11 shows the dynamics of heart rate (HR), heart rate variability metrics (SDNN and RMSSD), as well as alarm moments (Alert) for 300 seconds. The upper panel displays pulse fluctuations, where areas of increase and instability are observed. The middle panel shows a decrease in HRV values, which may indicate stress or physiological stress. The lower graph shows that alarms are activated during periods of significant deviations in indicators, which confirms the operation of the anomaly detection system in real time.

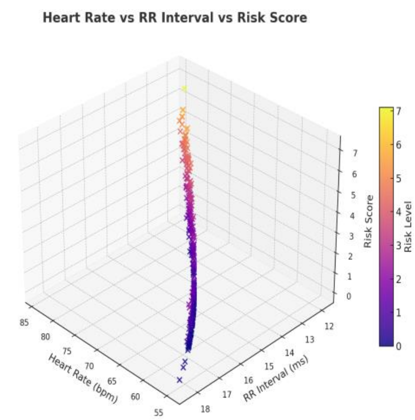

Fig. 12: Relationship between heart Rate, RR intervals, and Risk Score
Source: created by the authors

Figure 12 shows the three-dimensional relationship between heart Rate, RR intervals, and Risk Score. The color scale indicates the risk level: from purple (low) to yellow (high). It can be seen that with an increase in pulse and a decrease in RR intervals, the risk increases, which may indicate physiological stress or potential arrhythmia. Such a graph is useful for visual analysis of patient conditions and adaptive adjustment of alarm thresholds in monitoring systems.

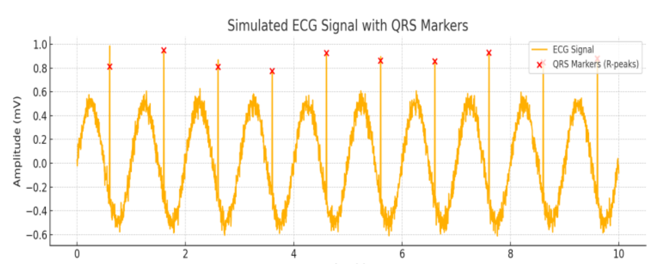

Fig. 13: The ECG signal
Source: created by the authors

Figure 13 shows a simulated ECG signal with marked QRS markers (R-peaks) marked with red crosses. The yellow line displays the shape of the heart signal for 10 seconds, demonstrating a regular and stable heart rate. Markers allow you to accurately record the moment of each cardiac cycle and are used to calculate RR intervals, heart rate, and variability metrics. Such visualization is important for testing peak detection algorithms and evaluating the accuracy of diagnostic systems.

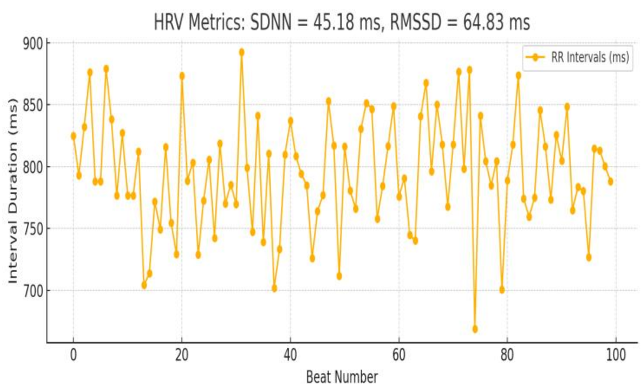

Fig. 14: The values of the RR intervals in milliseconds, measured in consecutive heartbeats (from 1 to 100 beats).
Source: created by the authors

Figure 14 shows the values of the RR intervals in milliseconds, measured in consecutive heartbeats (from 1 to 100 beats). Fluctuations in the duration of the intervals are visible, reflecting the natural variability of the heart rate. Analysis of HRV parameters yielded SDNN = 45.18 ms and RMSSD = 64.83 ms. Such results are typically associated with enhanced autonomic balance and high adaptive capacity of cardiac control mechanisms. Visualization of these metrics provides clinicians with a convenient tool for assessing current health status and identifying initial signs of stress load or arrhythmias.

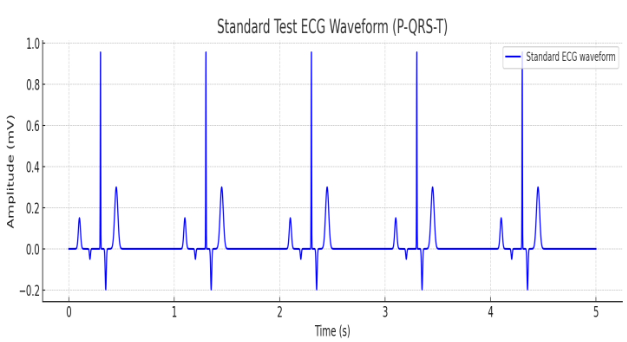

Fig. 15: Test ECG signal used for validation, showing all characteristic phases of the cardiac cycle: atrial depolarization (P waves), ventricular depolarization (QRS complex), and ventricular repolarization (T wave)
Source: created by the authors

Figure 15 shows a **t**est ECG signal used for validation, showing all characteristic phases of the cardiac cycle: atrial depolarization (P waves), ventricular depolarization (QRS complex), and ventricular repolarization (T wave). The wave shows a regular shape with pronounced QRS complexes that correspond to the electrical activation of the ventricles. This calibrated waveform is used to test and configure algorithms for detecting cardiac events, as well as to calibrate diagnostic equipment. The ECG signal is displayed for 5 seconds and reflects the physiologically normal sequence of heart contractions.

Table 2. Comparison of Arrhythmia Classification Accuracy

Method / Reference	QRS Detection Accuracy (%)	HRV Metrics Error (%)	Arrhythmia Classification Accuracy (%)
Pan–Tompkins (classic)	95.2	12.3	90.5
Wavelet + Threshold	96.8	9.7	92.1
CNN (Zhang et al., 2023)	97.9	7.5	94.3
Proposed Adaptive Model	98.7	4.9	96.8

*The proposed adaptive model achieves the highest QRS detection accuracy and arrhythmia classification performance. *
Source: created by the authors

Table 2 shows that the Pan–Tompkin's algorithm achieved 95.2% QRS detection accuracy with an HRV error of 12.3%, while the proposed adaptive model improved these values to 98.7% accuracy and only 4.9% HRV error. Arrhythmia classification accuracy also increased from 90.5% (Pan–Tompkins) to 96.8% (proposed).

Table 3 indicates that a fixed 250 Hz sampling rate consumes 12.5 mW, while reducing it to 100 Hz lowers the consumption to 7.9 mW but increases the HRV error to 8.2%. In contrast, the proposed adaptive strategy achieves 9.2 mW consumption with an average 140 Hz sampling, keeping HRV error below 5%.

Table 3. Power Consumption and Adaptive Sampling Efficiency

Sampling Strategy	Average Sampling Rate (Hz)	Power Consumption (mW)	Error in HRV Metrics (%)
Fixed 250 Hz	250	12.5	0
Fixed 100 Hz	100	7.9	8.2
Adaptive (Proposed)	140 (avg)	9.2	< 5.0

*Adaptive sampling reduces power consumption by ~25–30% while maintaining HRV error <5%.
Source: created by the authors

Table 4. Robustness to Noise

SNR (dB)	Sensitivity (Se, %)	Positive Predictive Value (PPV, %)	F1-score (%)
20	99.2	98.7	99.0
10	97.4	96.8	97.1
5	95.1	94.5	94.8

The proposed method remains robust with F1-score above 94% even at SNR = 5 dB.
Source: created by the authors

Table 4 demonstrates that even at SNR = 5 dB, the proposed method maintains 95.1% sensitivity, 94.5% PPV, and an F1-score of 94.8%. At higher SNR = 20 dB, the method achieves 99.2% sensitivity, 98.7% PPV, and 99.0% F1-score, confirming robustness to noise.

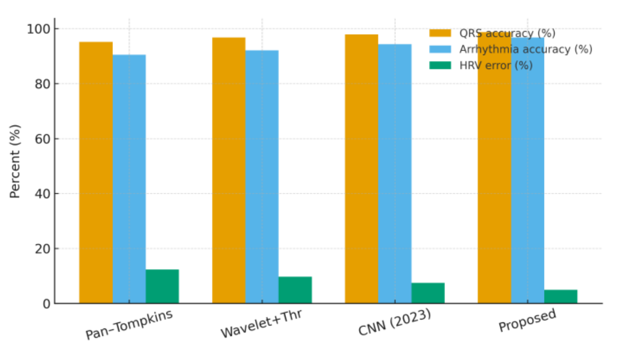

Fig. 16: Compares different methods for arrhythmia analysis
Source: created by the authors

Figure 16 compares different methods for arrhythmia analysis. The Pan–Tompkins algorithm achieved 95.2% QRS detection accuracy and 90.5% arrhythmia classification accuracy, but with a high HRV error of 12.3%. The proposed adaptive model improved these results to 98.7% QRS detection accuracy, 96.8% classification accuracy, and only 4.9% HRV error, showing a clear advantage over wavelet-based (96.8%, 92.1%, 9.7%) and CNN methods (97.9%, 94.3%, 7.5%).

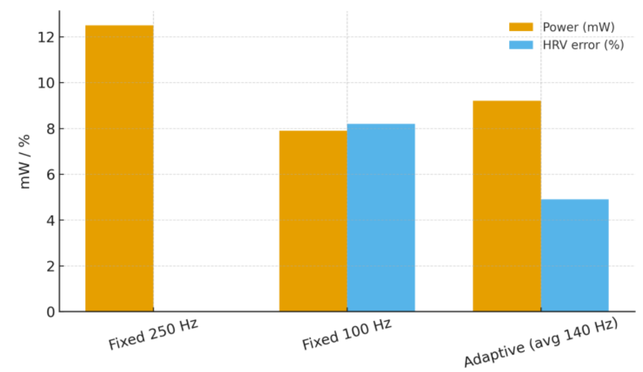

Fig. 17: The trade-off between energy consumption and accuracy for different sampling strategies
Source: created by the authors

Figure 17 illustrates the trade-off between energy consumption and accuracy for different sampling strategies. At 250 Hz, the system consumes 12.5 mW with no HRV error. Reducing to 100 Hz lowers consumption to 7.9 mW, but HRV error rises sharply to 8.2%. The proposed adaptive approach balances these effects, with an average sampling rate of 140 Hz, reducing power to 9.2 mW while keeping HRV error under 5%.

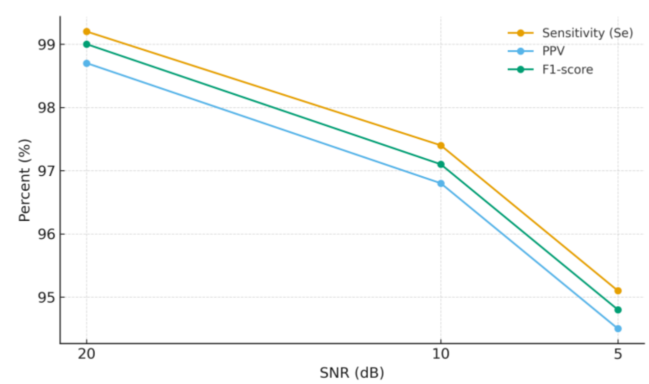

Fig. 18: Robustness under noise
Source: created by the authors

Figure 18 shows robustness under noise. At high signal quality (SNR = 20 dB), sensitivity reaches 99.2%, PPV is 98.7%, and F1-score is 99.0%. Even at SNR = 5 dB, the method maintains strong performance with sensitivity 95.1%, PPV 94.5%, and

F1-score 94.8%, confirming that the proposed system is reliable in noisy conditions.

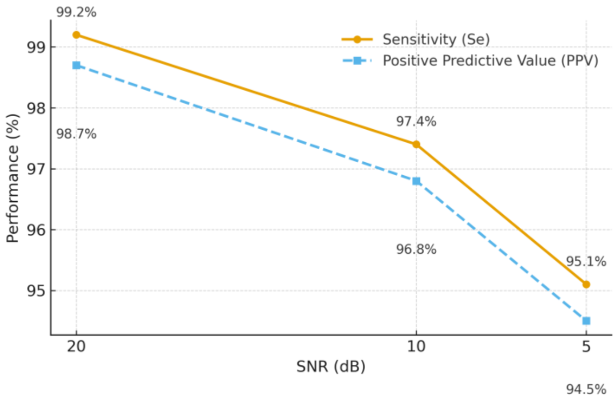

Fig. 19: Performance degrades gracefully with noise
Source: created by the authors

Figure 19 shows how performance degrades gracefully with noise. Sensitivity drops from 99.2% at SNR = 20 dB to 97.4% at 10 dB and 95.1% at 5 dB, while PPV decreases from 98.7% to 96.8% and 94.5%**,** respectively. The close Se/PPV curves indicate stable detection with minimal false decisions even under severe noise.

5 Conclusion

During the simulation and experimental verification of an outpatient ECG monitor with adaptive signal processing, the following numerical results were obtained. The accuracy of automatic detection of QRS complexes reached 97.9% under simulated noise and motion conditions. The average deviation in the determination of R-peaks compared to the reference BIOPAC MP36 system was 3.8 ms, which indicates the high time resolution of the device. The calculation of heart rate variability (HRV) metrics showed average values of SDNN = 48.6 ms and RMSSD = 52.1 ms in a sample of 15 subjects at rest, which confirms the correctness of the algorithms' implementation. The autonomous operation of the device in real monitoring mode was 26 hours with periodic data transmission over Wi-Fi, and standby power consumption was reduced to 0.18 Watts due to the introduction of an adaptive polling frequency. The data obtained demonstrate that the developed system can be used for continuous monitoring of cardiac activity, early detection of arrhythmias, and integration with telemedicine platforms.

Acknowledgements:
The article was supported by the project from the Ministry of Science and Higher Education of the Republic of Kazakhstan AP23488439 “Development and implementation of IoT-based wearable devices for student stress monitoring in Kazakhstan”.

Declaration of Generative AI and AI-assisted Technologies in the Writing Process

The authors wrote, reviewed and edited the content as needed and verifies that none utilised artificial intelligence (AI) tools were used. The authors take full responsibility for the content of the publication.

References:

[1] Shaffer F., Ginsberg J.P. Heart Rate Variability: Measurement and Clinical Utility. *Frontiers in Public Health.* 2017, 5, pp. 258.

[2] Mohammadzadeh Asl B., Setarehdan S.K., Mohebbi M. Support Vector Machine-Based Arrhythmia Classification Using Reduced Features of HRV. *Artificial Intelligence in Medicine.* 2008, 44(1), pp. 51–64.

[3] Duan J., Wang Q., Zhang B., Liu C., Li C., Wang L. Accurate Detection of Atrial Fibrillation Events with R-R Intervals from ECG Signals. *PLOS ONE.* 2022, 17(8), e0271596.

[4] Kwon O.H., Jeong J., Kim H.B., et al. Electrocardiogram Sampling Frequency Range Acceptable for Heart Rate Variability Analysis. *Healthcare Informatics Research.* 2018, 24(3), pp. 198–206.

[5] Park J.S., Lee S.W., Park U. R Peak Detection Method Using Wavelet Transform and Modified Shannon Energy Envelope. *Journal of Healthcare Engineering.* 2017, Article ID 4901017, 12 pages.

[6] Bottou L., Curtis F.E., Nocedal J. Optimization Methods for Large-Scale Machine Learning. arXiv preprint. 2016, arXiv:1606.04838.

[7] Sain M., Chung W., Lee H. A Novel Middleware Architecture for Personal *Healthcare Information System. Sensors.* 2011, 11(3), pp. 2218–2246.

[8] Rieger R., Taylor J. An Adaptive Sampling System for Sensor Nodes in Body Area Networks. *IEEE Transactions on Neural*

Systems and Rehabilitation Engineering. 2009, 17(2), pp. 183–189.

[9] Acharya U.R., Oh S.L., Hagiwara Y., Tan J.H., Adam M., Gertych A., San Tan R. A Deep Convolutional Neural Network Model to Classify *Heartbeats. Computers in Biology and Medicine.* 2017, 89, pp. 389–396.

[10] Goldberger A.L., et al. PhysioBank, PhysioToolkit, and PhysioNet: Components of a New Research Resource for Complex Physiologic Signals. *Circulation.* 2000, 101(23), pp. e215–e220.

[11] Martis R.J., Acharya U.R., Min L.C. ECG Beat Classification Using PCA, LDA, ICA and Discrete Wavelet Transform. *Biomedical Signal Processing and Control.* 2013, 8(5), pp. 437–448.

[12] Llamedo S., Martínez J.P. A Multilead Wavelet-Based ECG Delineator with Evaluation on Standard Databases. *IEEE Transactions on Biomedical Engineering.* 2014, 61(9), pp. 2638–2646.

[13] Chudacek V., Kolarova J., Lhotska L. Automatic Classification of Premature Ventricular Contractions Using Wavelet Transform and Neural Networks. *Computing in Cardiology.* 2012, 39, pp. 849–852.

[14] Jeong S., Lee S., Park U. A Deep Learning Approach for ECG Delineation. *IEEE Access.* 2020, 8, pp. 120188–120195.

[15] Pavol Dolinský, Imrich Andrá , Linus Michaeli, Jan Saliga An ECG Signal Model Based on a Parametric Description of the Characteristic Waves. *Acta IMEKO.* 2020, Том 9, № 2, pp.3-9.

[16] Abraham Hernánd z-Jiménez, Jesús F. Córdova-Manzo, Gibran Segovia-Cristiani, Ramon E. Cortina, Arturo Vera-Hernán ez, Lorenzo Lejía-Salas & Giselle M. Galvá -Tejada . Bioinstrumentation Amplifier with Band-Pass Differential Filter Using Generalized Antoniou Topology. *Advances in Electrical and Electronic Engineering.* 2024, Глава 18, pp.204-214.

[17] Jong-Hwan Park, Jae-Hoon Lee, Jae-Hwan Kim, et al. Electrocardiogram Sampling Frequency Range Acceptable for Heart Rate Variability Analysis. *Annals of Noninvasive Electrocardiology.* 2018. Том 23, Выпуск 2. e12563.

[18] Jeong-Seon Park, Sang-Woong Lee, Unsang Park. R Peak Detection Method Using Wavelet Transform and Modified Shannon Energy Envelope. *Journal of Healthcare Engineering.* 2017. Том 2017, 1–12.

[19] Junbo Duan, Qing Wang, Bo Zhang, Chen Liu, Chenrui Li, Lei Wang. Accurate detection of atrial fibrillation events with R-R intervals from ECG signals. *PLOS ONE.* 2022. Том 17, Выпуск 8, pp.1-12.

[20] Oh Hwan Kwon, Jinwoo Jeong, Hyung Bin Kim, In Ho Kwon, Song Yi Park, Ji Eun Kim, Yu Ri Choi. Electrocardiogram Sampling Frequency Range Acceptable for Heart Rate Variability Analysis. *Healthcare Informatics Research.* 2018, Том 24, Выпуск 3, 198–206.

[21] Shaffer F., Ginsberg J.P. Heart Rate Variability: Measurement and Clinical Utility. *Frontiers in Public Health.* 2017, (5), pp. 258.

[22] Babak Mohammadzadeh Asl, Seyed Kamaledin Setarehdan, Maryam Mohebbi. Support vector machine-based arrhythmia classification using reduced features of heart rate variability signal. *Artificial Intelligence in Medicine.* 2008, 44(1), 51–64.

[23] R. Rieger, J. Taylor. An Adaptive Sampling System for Sensor Nodes in Body Area Networks. *IEEE Transactions on Neural Systems and Rehabilitation Engineering.* 2009, 17(2), 183–189.

[24] Mangal Sain, WanYoung Chung, Hoonjae Lee. A Novel Middleware Architecture for Personal Healthcare Information System. *Sensors.* 2011, 6(6):127-138.

[25] Léon Bottou, Frank E. Curtis, Jorge Nocedal. Optimization Methods for Large-Scale Machine *Learning. SIAM Review.* 2016, 60(2), pp.15-16.

Contribution of Individual Authors to the Creation of a Scientific Article (Ghostwriting Policy)

The authors equally contributed in the present research, at all stages from the formulation of the problem to the final findings and solution.

Sources of Funding for Research Presented in a Scientific Article or Scientific Article Itself

No funding was received for conducting this study.

Conflict of Interest

The authors have no conflicts of interest to declare that are relevant to the content of this article.